



CHORUS

This is the accepted manuscript made available via CHORUS. The article has been published as:

Elucidating the magnetic and superconducting phases in the alkali metal intercalated iron chalcogenides

Meng Wang, Ming Yi, Wei Tian, Edith Bourret-Courchesne, and Robert J. Birgeneau

Phys. Rev. B **93**, 075155 — Published 29 February 2016

DOI: [10.1103/PhysRevB.93.075155](https://doi.org/10.1103/PhysRevB.93.075155)

Elucidating the magnetic and superconducting phases in the alkali metal intercalated iron chalcogenides

Meng Wang,^{1,*} Ming Yi,¹ Wei Tian,² Edith Bourret-Courchesne,³ and Robert J. Birgeneau^{1,3,4}

¹*Department of Physics, University of California, Berkeley, California 94720, USA*

²*Quantum Condensend Matter Division, Oak Ridge National Laboratory, Oak Ridge, Tennessee 37831, USA*

³*Materials Science Division, Lawrence Berkeley National Laboratory, Berkeley, California 94720, USA*

⁴*Department of Materials Science and Engineering, University of California, Berkeley, California 94720, USA*

The complex interdigitated phases have greatly frustrated attempts to document the basic features of the superconductivity in the alkali metal intercalated iron chalcogenides. Here, using elastic neutron scattering, energy-dispersive x-ray spectroscopy, and resistivity measurements, we elucidate the relations of these phases in $\text{Rb}_x\text{Fe}_y\text{Se}_{2-z}\text{S}_z$. We find: i) the iron content is crucial in stabilizing the stripe antiferromagnetic (AF) phase with rhombic iron vacancy order ($y \approx 1.5$), the block AF phase with $\sqrt{5} \times \sqrt{5}$ iron vacancy order ($y \approx 1.6$), and the iron vacancy-free phase ($y \approx 2$); ii) the iron vacancy-free superconducting phase ($z = 0$) evolves into an iron vacancy-free metallic phase with sulfur substitution ($z > 1.5$) due to the progressive decrease of the electronic correlation strength. Both the stripe AF phase and the block AF phase are Mott insulators. The iron-rich compounds ($y > 1.6$) undergo a first order transition from an iron vacancy disordered phase at high temperatures into the $\sqrt{5} \times \sqrt{5}$ iron vacancy ordered phase and the iron vacancy-free phase below T_s . Our data demonstrate that there are miscibility gaps between these three phases. The existence of the miscibility gaps in the iron content is a key to understanding the relationship between these complicated phases.

PACS numbers: 61.05.F-, 74.25.Dw, 74.25.F-, 74.70.Xa

I. INTRODUCTION

The discovery of superconductivity in the iron chalcogenides has generated a great deal of interest. The simplest PbO-type bulk FeSe superconducts below 8 K and 36.7 K under ambient and 8.9 GPa pressure, respectively, whereas single-layer FeSe films on a SrTiO_3 substrate have been reported to have superconducting (SC) transition temperatures (T_c) as high as 109 K¹⁻³. Intercalation of alkali-metals ($A = \text{Li}, \text{Na}, \text{K}, \text{Rb}, \text{and Cs}$) or a molecular spacer layer could enhance the T_c in bulk materials up to 46 K⁴⁻⁷. Most of the iron-based superconductors in bulk materials have been shown to be in the vicinity of an antiferromagnetically ordered parent compound. Furthermore, it has been found that the antiferromagnetic (AF) parent compounds could be progressively tuned to superconductors via carrier doping, isovalent doping, or pressure^{8,9}. Consequently, the AF ground state is viewed as one universal characteristic of the parent compounds in the iron pnictide and cuprate superconductors.

In the alkali-metal intercalated iron chalcogenide SC system, $A_x\text{Fe}_y\text{Se}_2$, a block AF order with large moments of $3.3\mu_B/\text{Fe}$, where μ_B is a Bohr magneton, and $\sqrt{5} \times \sqrt{5}$ iron vacancy order as presented in Fig. 1 ($x \approx 0.8$, $y \approx 1.6$, referred to as the 245 phase) always seems to be mesoscopically interdigitated with the SC phase that has been suggested to be an iron vacancy free phase in the studies to-date¹⁰⁻²³. The relationships between the two phases are still under debate. In addition, a stripe AF order that has the same magnetic structure as that in the iron pnictide parent materials albeit with additional rhombic iron vacancy order ($x \approx 1.0$, $y \approx 1.5$, referred

to as the 234 phase) and a phase with one Fe vacancy in eight Fe atoms ($x \approx 0.5$, $y \approx 1.75$, referred to as the 278 phase) have also been proposed as possible parent compounds^{24,25}. The complex mixture of phases is due to the difficulty in controlling the stoichiometry and separating the effect of many factors including the iron content, carrier doping, and isovalent substitution on the formation of the various phases and the T_c s²⁶⁻²⁹. Thus, it is crucial to identify the true parameters that tune between these phases including those responsible for inducing superconductivity, and then to compare these parameters between the iron pnictides and cuprates to elucidate the general relationship between magnetism and superconductivity.

For these purposes, we have synthesized different compositions of $\text{Rb}_x\text{Fe}_y\text{Se}_{2-z}\text{S}_z$ single crystals to study separately the effects of varying the Fe content and the Se:S ratio on the magnetic and superconducting phases. Firstly, we show that the 234 phase occurs at $y \approx 1.5$ and the 245 phase at $y \approx 1.6$ with a miscibility gap between them, regardless of the value of S concentration z . By varying y in the Fe content range $1.5 \leq y \leq 1.6$, both the 234 and 245 phases coexist, only the relative volume fractions of the two phases change as opposed to the characteristic structure of each phase. This necessitates that there is a miscibility gap between the two phases existing at $y \approx 1.5$ and 1.6.

For higher Fe content $y > 1.6$, while the 245 phase remains, the 234 phase is absent and an Fe vacancy-free phase ($y \approx 2$, referred to as the x22 phase) emerges. The relationship between the 245 phase and the x22 phase is exemplified by measurements on the nominal

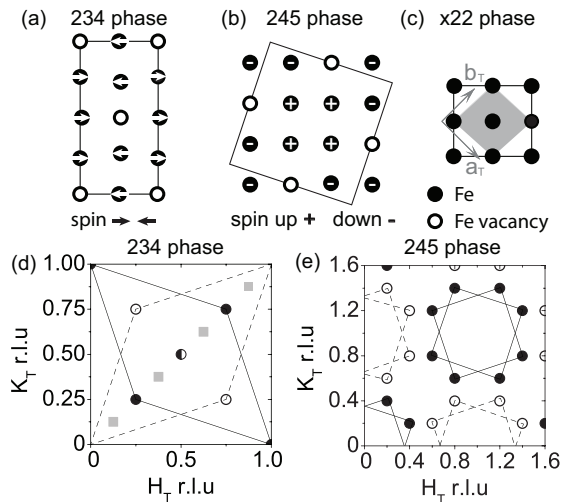


FIG. 1: (a) Schematics of an iron plane with in-plane ordered spins and rhombic iron vacancy order of the 234 phase^{24,30}, (b) the c -axis ordered spins and $\sqrt{5} \times \sqrt{5}$ iron vacancy order of the 245 phase^{10,31}, and (c) the iron vacancy-free x22 phase²². The shaded area in (c) represents the tetragonal unit cell we used. (d) The filled and open circles mark the wave vectors of reflection peaks associated with the 234 phase and (e) the 245 phase in the reciprocal space corresponding to the tetragonal unit cell that is used throughout the paper. The light gray squares in (d) show the wave vectors of a new set of peaks observed in $\text{Rb}_{0.8}\text{Fe}_{1.5}\text{Se}_2$.

$\text{Rb}_{0.8}\text{Fe}_2\text{S}_2$ compound, where a single phase with randomly distributed iron vacancies at high temperatures is observed to go through a first order transition to phase separate into the 245 phase and the x22 phase. The first order nature of the structural transition and the significantly different bond lengths of the two phases suggest the existence of another miscibility gap between the 245 phase and the x22 phase at $y \approx 1.6$ and 2.

In addition, we show that for high Fe content, the Se:S ratio tunes the vacancy-free x22 phase from a metallic phase to a superconducting phase. Hence we have arrived at a phase diagram where the Fe content is identified as the key parameter in tuning between and stabilizing the insulating and metallic phases, while the Se:S ratio is important for inducing superconductivity from the non-magnetic metallic phase of $\text{Rb}_x\text{Fe}_2\text{S}_2$.

The rest of the paper is organized as follows. In Sec. II, we introduce the experimental techniques and samples that have been used in this paper. Section III presents all the experimental results, with subsection A the neutron diffraction data on nominal compositions of $\text{Rb}_{0.8}\text{Fe}_{1.5}\text{Se}_2$, $\text{Rb}_{0.8}\text{Fe}_{1.5}\text{SeS}$, and $\text{Rb}_{0.8}\text{Fe}_2\text{S}_2$ single crystals, and subsection B the resistivity measurements on a series of nominal compositions of $\text{Rb}_{0.8}\text{Fe}_y\text{Se}_{2-z}\text{S}_z$, $y = 1.5$ and 2, $0 \leq z \leq 2$ samples. In Sec. IV, we present the phase diagrams resulting from our measurements and discuss the relationships of the various magnetic and superconducting phases found in $\text{Rb}_x\text{Fe}_y\text{Se}_{2-z}\text{S}_z$. Section V briefly summarizes the major conclusions of this paper

and presents a comparison with the iron pnictide superconductors.

II. EXPERIMENTS

We carried out the neutron scattering experiments on the HB-1A triple axis spectrometer at the High-Flux Isotope Reactor, Oak Ridge National Laboratory. Details about the single crystal growth and configurations of neutron scattering experiments have been described elsewhere³⁰. The samples used for neutron scattering experiments are 0.5, 0.7 and 0.3 g for $\text{Rb}_{0.8}\text{Fe}_{1.5}\text{Se}_2$, $\text{Rb}_{0.8}\text{Fe}_{1.5}\text{SeS}$, and $\text{Rb}_{0.8}\text{Fe}_2\text{S}_2$, respectively. The resistivity measurements using the standard four probe method with a physical property measurement system (PPMS) from Quantum Design Inc. have been performed on single crystals with a typical size of $0.5 \times 2 \times 4 \text{ mm}^3$. The electron beam for the energy-dispersive x-ray spectroscopy (EDX) was fixed at 20.0 KeV. The errors of the compositions determined by EDX can be up to 8%, which could be ascribed to the inhomogeneous distribution of two coexisting phases. All the measurements have been performed on single crystals. The samples used for neutron scattering experiments are from the same batches as the resistivity measurements for the same compounds. We list in Table I the samples measured in this paper and reported previously that have been taken into consideration to make the conclusions here.

TABLE I: The nominal and actual compositions and phases of samples we have measured in the $\text{Rb}_x\text{Fe}_y\text{Se}_{2-z}\text{S}_z$ system.

nominal	actual composition	phases	Ref.
	—	234, 245	30
$\text{Rb}_{0.8}\text{Fe}_{1.5}\text{S}_2$	$\text{Rb}_{0.66}\text{Fe}_{1.36}\text{S}_2^*$	234	32
	$\text{Rb}_{0.78}\text{Fe}_{1.35}\text{S}_2^\dagger$	234	
$\text{Rb}_{0.8}\text{Fe}_{1.5}\text{Se}_2$	$\text{Rb}_{0.93}\text{Fe}_{1.38}\text{Se}_2^\ddagger$	234, 245	
$\text{Rb}_{0.8}\text{Fe}_{1.5}\text{SeS}$	$\text{Rb}_{0.55}\text{Fe}_{1.53}\text{Se}_{1.25}\text{S}_{0.75}^\ddagger$	234, 245	this work
$\text{Rb}_{0.8}\text{Fe}_2\text{S}_2$	$\text{Rb}_{0.75}\text{Fe}_{1.85}\text{S}_2^\ddagger$	245, x22	
$\text{Rb}_{0.8}\text{Fe}_2\text{Se}_{2-z}\text{S}_z$ $z = 0, 1, 1.25, 1.5$	—	245, x22	
$\text{Rb}_{0.8}\text{Fe}_2\text{Se}_2$	$\text{Rb}_{0.75}\text{Fe}_{1.63}\text{Se}_2^*$	245, x22	31
$\text{Rb}_{0.8}\text{Fe}_{1.6}\text{Se}_2$	$\text{Rb}_{0.89}\text{Fe}_{1.58}\text{Se}_2^*$	245	

* refined by neutron powder diffraction.

† refined by neutron single crystal diffraction.

‡ determined by EDX.

* determined by inductively coupled plasma atomic emission spectroscopy (ICP).

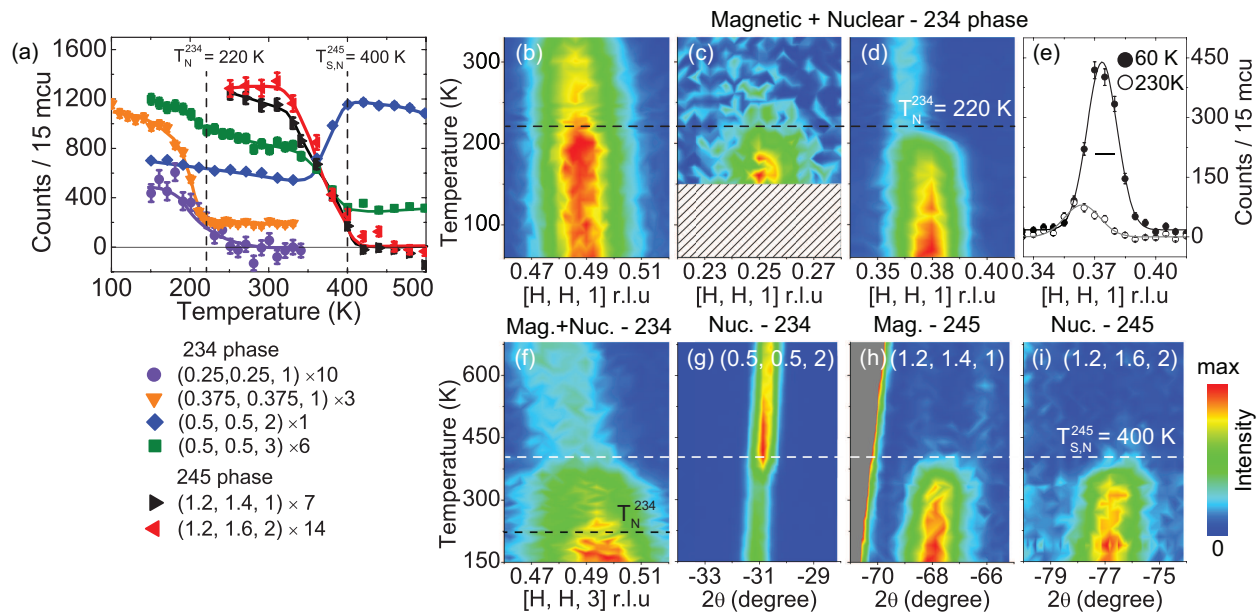


FIG. 2: (Color online). (a) Temperature dependence of the peak intensities in $\text{Rb}_{0.8}\text{Fe}_{1.5}\text{Se}_2$. The intensities for each peak have been normalized by a factor as shown following the corresponding wave vector. (b)-(f) The magnetic and superlattice peaks of the 234 phase scanned along the $[H, H, 1]$ direction and (f) the $[H, H, 3]$ direction. The bar in (e) indicates the instrumental resolution. (g) $\theta - 2\theta$ scans of the rhombic iron vacancy order for the 234 phase at $Q = (0.5, 0.5, 2)$ as a function of temperature. (h) $\theta - 2\theta$ scans of the 245 phase through the magnetic peak $Q = (1.2, 1.4, 1)$ and (i) the $\sqrt{5} \times \sqrt{5}$ iron vacancy ordered peak $Q = (1.2, 1.6, 2)$. The black and white dashed lines mark the Néel temperature of the 234 phase at $T_N^{234} = 220$ K and the coincidental magnetic and structure transition temperature of the 245 phase at $T_{s,N}^{245} = 400$ K, respectively. The intensities in (b-i) have been normalized for better comparison. The lattice constants are chosen as the average of the two phases with $a = b = 3.991$ Å and $c = 14.017$ Å in the tetragonal notation optimized at 60 K. The ‘mcu’ in units of intensity is a defined monitor count unit, which we defined as $1 \text{ mcu} \approx 1$ second.

III. RESULTS

A. Neutron diffraction measurements

1. $\text{Rb}_{0.8}\text{Fe}_{1.5}\text{Se}_2$

We first present neutron diffraction data in Fig. 2 for the insulating compound with nominal composition of $\text{Rb}_{0.8}\text{Fe}_{1.5}\text{Se}_2$, in which both the 234 phase and the 245 phase coexist^{24,30}. We plot the peak intensities at wave vectors associated with the 234 phase as a function of temperature in Fig. 2(a) and color maps in Figs. 2(b)-2(g). The results demonstrate that the 234 phase exists in this compound with a Néel temperature of $T_N = 220$ K [Figs. 2(a)-2(e)]. The rhombic iron vacancy order of the 234 phase exists at all the temperatures we measured³⁰, as signals in Fig. 2(g). In addition, we find another set of peaks at $H = 1/8, 3/8, 5/8$, and $7/8$ in the $[H, H, L]$ plane, where $L = \text{odd}$. The peak heights at $H = 3/8, 5/8$, and $7/8$ in the $[H, H, 1]$ scattering plane follow the trend of $|\mathbf{S}_\perp|^2 F(\mathbf{Q})^2$, where \mathbf{S}_\perp is the component of the in-plane ordered moments perpendicular to the momentum transfer \mathbf{Q} and $F(\mathbf{Q})$ is the magnetic form factor of Fe^{2+} , demonstrating that the peaks are magnetic. The temperature dependence of the peak intensity at $Q = (3/8, 3/8, 1)$ shows a transition at $T_N^{234} = 220$ K,

suggesting that the new set of peaks has the same magnetic origin as the stripe AF order. One possible explanation is that the 234 phase exhibits a super iron vacancy order in addition to the rhombic iron vacancy order. The residual intensities at $Q = (0.5, 0.5, 1)$ in Fig. 2(b) above 220 K and the transition-like behavior in the peak intensities at $Q = (0.5, 0.5, 3)$ at 400 K are consistent with a model in which the peak intensities have a combination of contributions from the nuclear reflection of the super iron vacancy order and a $\sqrt{2} \times \sqrt{2}$ Rb vacancy order between 220 K and 400 K, and a pure $\sqrt{2} \times \sqrt{2}$ Rb vacancy order at temperatures above 400 K^{13,31,33}.

Figures 2(a), 2(h), and 2(i) demonstrate that the 245 phase with simultaneous magnetic and iron vacancy order-disorder transitions at $T_{s,N} = 400$ K also coexists in this composition.

Kinks are clearly observed in the intensities of the peaks associated with the 234 phase at the transition temperature $T_{s,N} = 400$ K of the 245 phase, as shown in Figs. 2(f)-2(i), demonstrating the mobility of the iron vacancies between the two phases. It is possible that the free iron ions released from the iron vacancy disordered 245 phase at temperatures above $T_{s,N} = 400$ K occupy the vacant sites that form the super iron vacancy order. As a result, the peak intensities at $Q = (0.5, 0.5, 3)$ decrease at temperatures above $T_s = 400$ K, and conversely,

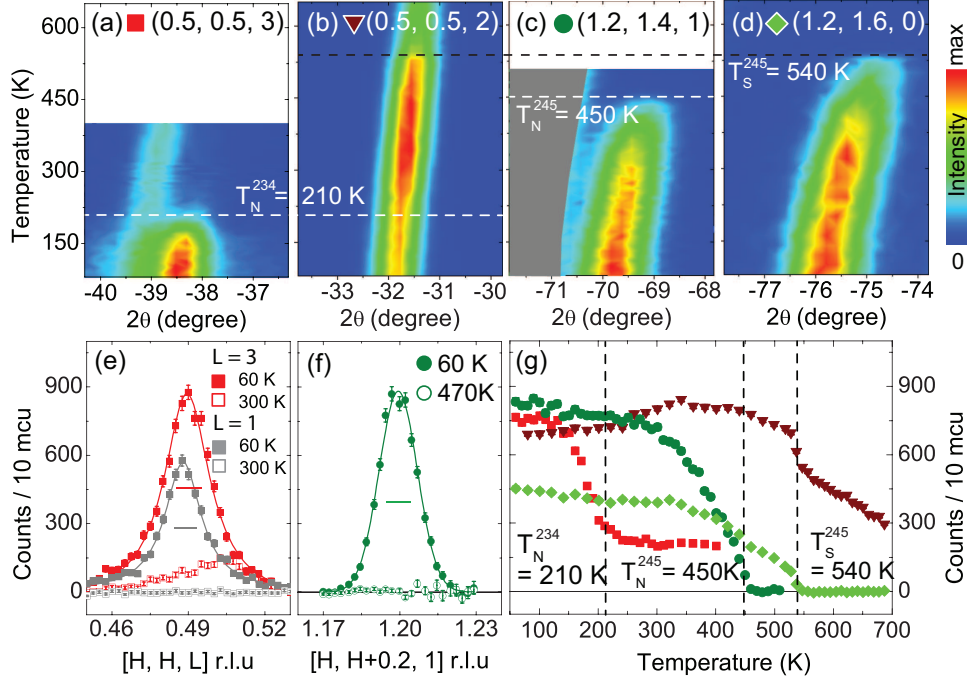


FIG. 3: (Color online). Temperature dependence of neutron diffraction peaks in insulating $\text{Rb}_{0.8}\text{Fe}_{1.5}\text{SeS}$. (a) $\theta - 2\theta$ scans of the magnetic peak at $Q = (0.5, 0.5, 3)$ and (b) the rhombic iron vacancy ordered peak at $Q = (0.5, 0.5, 2)$. The white dashed lines at $T = 210$ K in (a) and (b) mark the Néel temperature of the 234 phase. (c) $\theta - 2\theta$ scans of the magnetic peak at $Q = (1.2, 1.4, 1)$ and (d) the $\sqrt{5} \times \sqrt{5}$ iron vacancy ordered peak at $Q = (1.2, 1.6, 0)$ of the 245 phase. The grey area in (c) blocks a spurious peak of Al. (e) Scans through the magnetic peaks associated with the 234 phase at $Q = (0.5, 0.5, L = 1$ and $3)$ at 60 K and 300 K along the $[H, H, L]$ directions and (f) the magnetic peak associated with the 245 phase at $Q = (1.2, 1.4, 1)$ at 60 K and 470 K along the $[H, H + 0.2, 1]$ direction, respectively. The lattice constants are chosen as the average of the two phases with $a = b = 3.846$ Å and $c = 14.188$ Å in the tetragonal notation. (g) Order parameters of the magnetic (red squares) and rhombic iron vacancy order (brown triangles) of the 234 phase, and the $\sqrt{5} \times \sqrt{5}$ iron vacancy order (light green diamonds) and the block AF order (dark green circles) of the 245 phase, respectively. The intensities in (g) are obtained by fitting the heights of the peaks in (a)-(d).

the peak at $Q = (0.5, 0.5, 2)$ that represents the rhombic iron vacancy order is enhanced, as seen in Figs. 2(a), 2(f), and 2(g). The weak Bragg peaks of the 245 phase presented in Fig. 2(a) indicate that the 245 phase has a small volume fraction, consistent with the low iron content revealed by EDX and the existence of a super iron vacancy order in addition to the rhombic iron vacancy order.

We calculate the spin correlation length ξ by the Fourier transform from reciprocal space to real space, resulting in $\xi = 8\ln 2/q_{FWHM}$. The q_{FWHM} is the full-width-half-maximum (FWHM) of the peak in units of Å⁻¹. The peak in Fig. 2(e) is fitted as a Gaussian function $I = I_0 \exp[-(H - H_0)^2 / (2\sigma^2)]$. The FWHM of the observed peak $H_{obs} = 2\sqrt{2\ln 2}\sigma = \sqrt{H_{res}^2 + H_{int}^2}$, where H_{res} is the instrumental resolution and H_{int} is the intrinsic broadening of the spin-spin correlation to the FWHM of the reflection peak³⁴. For scans along the $[H, H]$ direction, the $q_{FWHM} = 2\pi\sqrt{(H_{int}/a)^2 + (K_{int}/b)^2} = 2\sqrt{2}\pi H_{int}/a$. We have $\xi_{234} = [2\sqrt{2\ln 2}/\pi](a/H_{int}) = 150 \pm 5$ Å. A similar calculation based on the scan along the $[H, H + 0.2, 1]$ direction at $Q = (1.2, 1.4, 1)$ (not

shown) yields a spin correlation length of the 245 phase $\xi_{245} = 93 \pm 9$ Å. The finite spin correlation lengths suggest that the 234 phase and the 245 phase are separated on a mesoscopic scale in $\text{Rb}_{0.8}\text{Fe}_{1.5}\text{Se}_2$.

2. $\text{Rb}_{0.8}\text{Fe}_{1.5}\text{SeS}$

Neutron diffraction data of a single crystal with nominal composition $\text{Rb}_{0.8}\text{Fe}_{1.5}\text{SeS}$ are presented in Fig. 3. The data confirm the existence of the 234 phase with a Néel temperature of $T_N = 210$ K and the 245 phase with separated phase transition temperatures of $T_N = 450$ K and $T_s = 540$ K. The scans through the magnetic peaks of the 234 phase at $Q = (0.5, 0.5, L = 1$ and $3)$ in Fig. 3(e) yield a spin correlation length of $\xi_{234} = 130 \pm 7$ Å for $L = 1$, and $\xi_{234} = 115 \pm 5$ Å for $L = 3$ at 60 K. An estimation based on the scan at $Q = (1.2, 1.4, 1)$ as shown in Fig. 3(f) reveals a spin correlation length $\xi_{245} = 166 \pm 8$ Å for the 245 phase at 60 K. The order parameters obtained from Figs. 3(a)-3(d) are presented in Fig. 3(g). These data suggest that the volume frac-

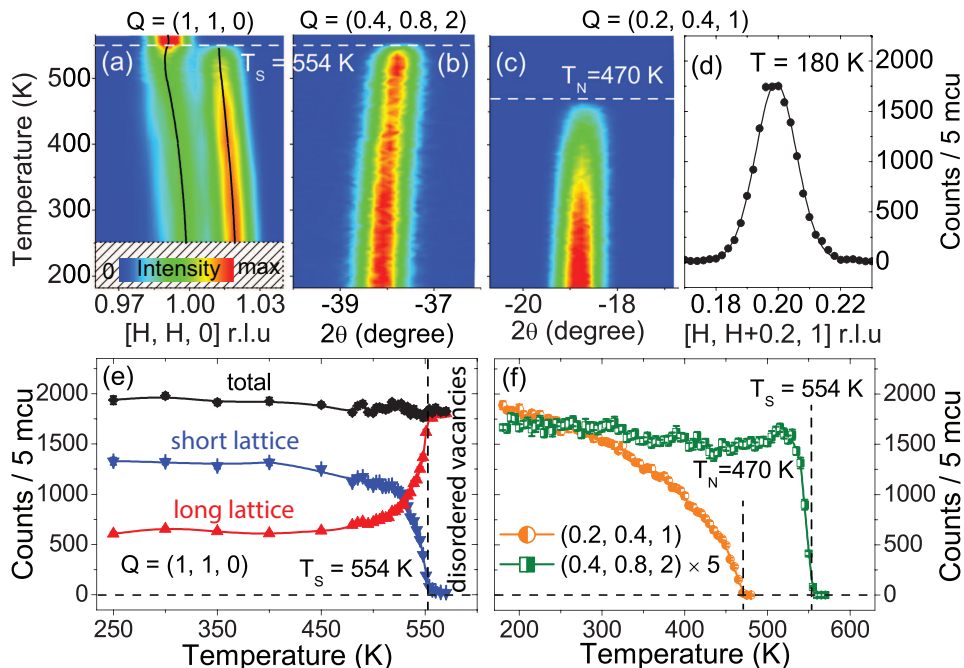


FIG. 4: (Color online). Temperature dependence of neutron diffraction peaks in metallic $\text{Rb}_{0.8}\text{Fe}_2\text{S}_2$. (a) Two well-separated peaks at $Q = (1, 1, 0)$ along the $[H, H, 0]$ direction. The left peak is associated with the 245 phase that has the lattice constants of $a = b = 3.782 \text{ \AA}$ at 250 K, and the iron vacancy disordered phase with $a = b = 3.811 \text{ \AA}$ at 570 K. The right peak belongs to the metallic phase with shorter lattice constants of $a = b = 3.705 \text{ \AA}$ at 250 K. (b) $\theta - 2\theta$ scans through the $\sqrt{5} \times \sqrt{5}$ iron vacancy ordered peak at $Q = (0.4, 0.8, 2)$ and (c) the block AF ordered peak at $Q = (0.2, 0.4, 1)$ of the 245 phase. (d) A magnetic peak scan through $Q = (0.2, 0.4, 1)$ along the $[H, H+0.2, 1]$ direction at 180 K. (e) The blue and red triangles are peak intensities extracted from the right and left peaks in (a), respectively. The black diamond is a sum of the two at each temperature. At temperatures above $T_s = 554 \text{ K}$, the two phases merge into an iron vacancy disordered phase. (f) Temperature dependence of the peak heights obtained from (b) and (c), respectively, which shows the Néel temperature at $T_N = 470 \text{ K}$ and the iron vacancy order-disorder transition temperature at $T_s = 554 \text{ K}$. The intensities of the peak at $Q = (0.4, 0.8, 2)$ have been multiplied by a factor of 5 in (b) and (f) for comparison.

tions of the two phases are comparable. In contrast to the measurements in $\text{Rb}_{0.8}\text{Fe}_{1.5}\text{Se}_2$, we did not observe any reflection peaks indicative of the existence of a super iron vacancy order. The 234 and 245 phases are each found in $\text{Rb}_{0.8}\text{Fe}_{1.5}\text{Se}_2$, $\text{Rb}_{0.8}\text{Fe}_{1.5}\text{SeS}$, and the previously studied $\text{Rb}_{0.8}\text{Fe}_{1.5}\text{S}_2$ (Ref. 30). This implies that the Se:S ratio does not affect the formation of the iron vacancy ordered phases.

3. $\text{Rb}_{0.8}\text{Fe}_2\text{S}_2$

To elucidate the role of the iron content, we carried out additional neutron diffraction measurements on the crystal with nominal composition of $\text{Rb}_{0.8}\text{Fe}_2\text{S}_2$. The diffraction data are presented in Fig. 4. Scans at $Q = (1, 1, 0)$ show two well separated peaks below 554 K [Fig. 4(a)]. Measurements at the wave vectors associate with the 245 phase in Fig. 4(b) and Fig. 4(c) confirm the presence of the 245 phase with a Néel temperature of $T_N = 470 \text{ K}$ and a structural transition temperature of $T_s = 554 \text{ K}$. Using the set of parameters $a = b = 3.782 \text{ \AA}$ and $c = 14.029 \text{ \AA}$ the magnetic peak of the 245 phase at

$Q = (0.2, 0.4, 1)$ is well centered at $H = 0.2$ along the $[H, H + 0.2, 1]$ direction at 180 K, as shown in Fig. 4(d). Thus, we identify the left peak in Fig. 4(a) centered at $Q = (1, 1, 0)$ as associated with the 245 phase. The 245 phase as a tetragonal structure should not result in an extra peak at $Q = (1, 1, 0)$ ¹⁰. From the metallic behavior exhibited in transport and ARPES measurements on the same compound³⁵, we identify that the right peak at $Q = (1, 1, 0)$ in Fig. 4(a) belongs to a metallic phase with the shorter in-plane lattice constant of $a = b = 3.705 \text{ \AA}$ at 250 K. Within the instrumental resolution, we could not distinguish the difference in the lattice constants along the c axis.

The phase with shorter in-plane lattice constant is attributed to one with fewer iron vacancies. The significantly shortened lattice of the metallic phase suggests that it is likely an iron vacancy-free phase. The metallic phase is approximately 67% in volume as estimated from the intensities of the peaks at $Q = (1, 1, 0)$. The volume fraction ratio of the two phases and the averaged composition of $\text{Rb}_{0.75}\text{Fe}_{1.85}\text{S}_2$ also implies that the 245 phase stabilizes at $y \approx 1.6$ and the metallic phase is iron vacancy-free with $y \approx 2$. The two phases merge

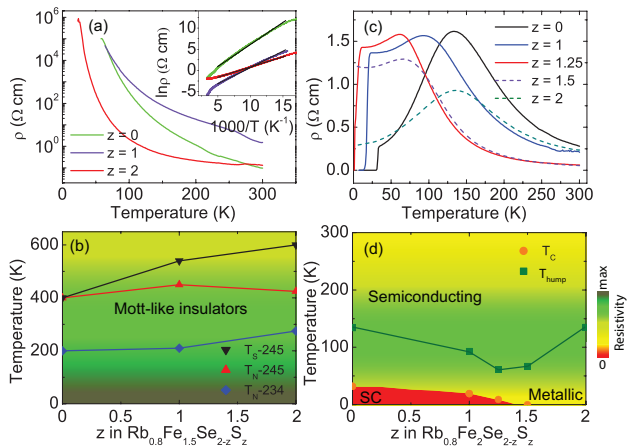


FIG. 5: (Color online). (a) In-plane resistivity measurements of insulating $\text{Rb}_{0.8}\text{Fe}_{1.5}\text{Se}_{2-z}\text{S}_z$ with $z = 0, 1$, and 2 . The inset shows resistivity in log scale plotted against $1000/T$, along with fits of $\rho = \rho_0 \exp(E_a/k_B T)$. (b) A phase diagram of insulating $\text{Rb}_{0.8}\text{Fe}_{1.5}\text{Se}_{2-z}\text{S}_z$ as a function of sulfur doping. The solid lines mark the Néel temperatures of the 234 phase (blue), the 245 phase (red) and the $\sqrt{5} \times \sqrt{5}$ iron vacancy order-disorder transition (black). (c) Resistivity measurements for $\text{Rb}_{0.8}\text{Fe}_2\text{Se}_{2-z}\text{S}_z$ with $z = 0, 1, 1.25, 1.5$ and 2 . (d) A phase diagram of $\text{Rb}_{0.8}\text{Fe}_2\text{Se}_{2-z}\text{S}_z$ as a function of sulfur doping. The T_c s and T_{hump} s are extracted from (c). The color in (b) and (d) indicates the magnitude of resistivity.

with increasing temperature into a single iron vacancy disordered phase at temperatures just above $T_s = 554$ K, as shown in Figs. 4(a), 4(b), and 4(e). The $\sqrt{2} \times \sqrt{2}$ Rb vacancy order that has been observed in superconducting $\text{Rb}_{0.75}\text{Fe}_{1.63}\text{Se}_2$ (Ref. 31) is not observed in $\text{Rb}_{0.75}\text{Fe}_{1.85}\text{S}_2$. We searched but did not find any evidence for the existence of the 234 phase in this compound.

B. Resistivity measurements

1. $\text{Rb}_{0.8}\text{Fe}_{1.5}\text{Se}_{2-z}\text{S}_z$, $0 \leq z \leq 2$

The results of measurements of the resistivity on samples with nominal compositions of $\text{Rb}_{0.8}\text{Fe}_{1.5}\text{Se}_{2-z}\text{S}_z$, $z = 0, 1, 2$, are presented in Fig. 5 (a). All of the resistivity curves turn up at low temperatures, indicating insulating behaviors. In the inset, we show the results of fits of the resistivity data to the form $\rho = \rho_0 \exp(E_a/k_B T)$, where k_B is the Boltzmann constant and E_a is the thermal activation gap³⁶, resulting in $E_a = 89.5 \pm 0.5, 66.1 \pm 0.4$, and 41.1 ± 0.2 meV for $z = 0, 1$, and 2 , respectively. Consistent with previous measurements, the thermal activation gaps^{24,30,36} are much smaller than the band gaps that are measured directly by ARPES for both the 234 phase and the 245 phase^{12,32}, which could be due to the pressure effect on the internal interfaces or alternatively the existence of a small undetectable quasiparticle spectral weight near the Fermi energy. A phase diagram with the

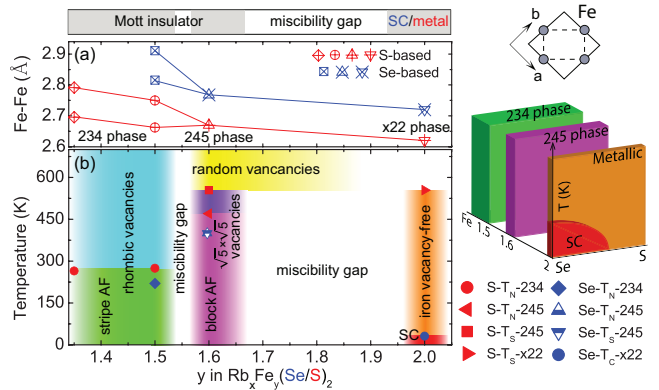


FIG. 6: (Color online). (a) Fe-Fe bond lengths of the 234 phase, the 245 phase, and the “x22” phase for the S-based (red) and Se-based (blue) materials. The upper inset on the right is a sketch showing the Fe-Fe bonds along the two directions and the unit cell used throughout the paper marked by the solid line. (b) A phase diagram of temperature versus the iron content y in $\text{Rb}_x\text{Fe}_y(\text{Se}/\text{S})_2$. The red and blue points are associated with the sulfide and selenide compounds, respectively. The white areas are miscibility gaps. The point at $y = 1.35$ is obtained from previous work³². The lower inset on the right is a schematic three-dimensional phase diagram with temperature, iron content, and Se:S ratio.

transition temperatures of the two phases obtained from neutron diffraction experiments is given in Fig. 5(b).

2. $\text{Rb}_{0.8}\text{Fe}_2\text{Se}_{2-z}\text{S}_z$, $0 \leq z \leq 2$

In Fig. 5(c), we show the results of resistivity measurements on various nominal compositions of $\text{Rb}_{0.8}\text{Fe}_2\text{Se}_{2-z}\text{S}_z$ single crystals below 300 K. The T_c s are gradually suppressed from 32 K ($z = 0$)³⁷ to 20 K ($z = 1$) to 9 K ($z = 1.25$) and 0 K ($z = 1.5$) by sulfur substitution. Humps in the resistivity (T_{hump}) appear between 75 K and 150 K. The compounds are semiconducting for $T > T_{hump}$, and become superconducting or metallic for $T < T_{hump}$. The pure $\text{Rb}_{0.8}\text{Fe}_2\text{S}_2$ crystal is clearly metallic from the resistivity curve in Fig. 5(c) and the band structure measurements by ARPES³⁵, in contrast to a previous report showing a semiconducting behavior³⁸; the latter could be caused by iron content deviations. The metallic characteristic in $\text{Rb}_{0.8}\text{Fe}_2\text{S}_2$ is consistent with the observation of the iron vacancy-free phase in neutron diffraction measurements, as shown in Figs. 4(a) and 4(e). These observations result in a phase diagram as shown in Fig. 5(d), suggesting that the metallic phase in $\text{Rb}_{0.8}\text{Fe}_2\text{S}_2$ is continuously connected to the SC phase in $\text{Rb}_{0.8}\text{Fe}_2\text{Se}_2$ as S is progressively replaced by Se. The commonly observed 245 phase exists in all the nominal compositions of $\text{Rb}_{0.8}\text{Fe}_2\text{Se}_{2-z}\text{S}_z$ as a mesoscopically separated phase. Note that the Fe content is in fact less than 2 which means that all of the samples are in the two phase coexistence region^{11–23}.

IV. DISCUSSION

A. The effect of iron content

For lower Fe content, $y < 1.6$, our results demonstrate that the rhombic iron vacancy ordered phase is energetically stable for compositions with iron content $y \leq 1.5$. The associated stripe AF order forms at temperatures below the Néel temperature of the 234 phase. The pure stripe phase is achieved in samples with a refined composition of $\text{Rb}_{0.78}\text{Fe}_{1.35}\text{S}_2$ (Ref. 32). In the regime $1.5 < y < 1.6$, both the rhombic iron vacancy order and the $\sqrt{5} \times \sqrt{5}$ iron vacancy order coexist mesoscopically, while only the ratio of the volume fraction of the two phases varies³⁰, suggesting the existence of a miscibility gap. The two phases are both characterized as Mott insulators with large gaps at the Fermi level and localized electrons, promoted by the iron vacancies, as well as a high spin configuration, $S = 2$ ^{12,39–41}. For higher Fe content, $y > 1.6$, as exemplified by the first order structural transition in nominal composition of $\text{Rb}_{0.8}\text{Fe}_2\text{S}_2$ at $T_s = 554$ K, and the distinct Fe-Fe bond distances [Fig. 6(a)], as well as the iron contents in the 245 phase and the metallic phase imply the existence of another miscibility gap in y between the two phases at temperatures below T_s . Adjusting the additional iron in the starting mixtures does not extend the miscibility gap⁴². The temperature dependences of the phase transitions in $\text{Rb}_{0.8}\text{Fe}_2\text{S}_2$ are in good agreement with those of the SC phase in $A_x\text{Fe}_y\text{Se}_2$ ^{22,43}.

The effects of disorder are always more significant in quenched samples and at interfaces. Not surprisingly, some compositions within the miscibility gaps are reported in quenched samples. A scanning tunneling microscopy study reveals a 278 phase with $y = 1.75$ in some areas of SC $\text{K}_x\text{Fe}_y\text{Se}_2$ (Ref. 25). The 278 phase is more likely a surface state, since it has not been observed in bulk materials studied over a wide range of compositions. Neutron diffraction studies on a nonsuperconducting (NSC) $\text{Rb}_x\text{Fe}_{2-y}\text{Se}_2$ compound also identify a NSC phase with a composition of $\text{Rb}_{0.92}\text{Fe}_{1.81}\text{Se}_2$, containing interdigitated 234 and 245 phase²³. However, a superconducting transition has been realized in an annealed NSC sample⁴⁴. All these observations are consistent with the existence of the miscibility gaps in the phase diagram in equilibrium bulk materials.

B. The effect of Se:S ratio

The replacement of selenium by sulfur does not affect the structures and the insulating ground states for the 234 phase and the 245 phase. However, it progressively decreases the superconducting transition temperature of the iron vacancy-free phase and results in the metallic phase in $\text{Rb}_{0.8}\text{Fe}_2\text{S}_2$. The absence of superconductivity in $\text{Rb}_{0.8}\text{Fe}_2\text{S}_2$ is due to the extended overall bandwidth compared to those in SC $\text{Rb}_{0.8}\text{Fe}_2\text{Se}_2$, presumably

caused by the smaller sulfur ions, the decreased electronic correlation³⁵, and the shorter Fe-Fe bond lengths as plotted in Fig. 6(a). As revealed in the three dimensional phase diagram in Fig. 6, there are two first order transitions between the stripe AF phase and the superconducting phase; isovalent substitution of selenium on the sulfur sites induces superconductivity from a nonmagnetic metallic phase. These are in clear contrast to the effects of isovalent phosphorus doping on the arsenic sites in BaFe_2As_2 , where the superconductivity emerges continuously from an antiferromagnetic parent compound^{8,9}.

C. The interplay of the phases

Neutron^{22,23} and synchrotron x-ray¹⁹ diffraction, together with NMR¹⁷ studies on superconducting $A_x\text{Fe}_y\text{Se}_2$ reveal that the SC phase is nearly iron vacancy-free ($y \approx 2$) with x spanning between 0.3 and 0.58. Due to the existence of the $\sqrt{5} \times \sqrt{5}$ iron vacancy ordered phase, the macroscopically averaged iron contents of the two phases below T_s and the iron vacancy randomly distributed phase above T_s are always less than $y = 2$. The simultaneous appearance of the x22 phase and the $\sqrt{5} \times \sqrt{5}$ iron vacancy order explains the reason that the 245 phase always accompanies the superconducting phase in $A_x\text{Fe}_y\text{Se}_{2-z}\text{S}_z$.

V. CONCLUSION

Our studies on a comprehensive range of samples in the $\text{Rb}_x\text{Fe}_y\text{Se}_{2-z}\text{S}_z$ compounds result in the phase diagrams shown in Fig. 6. By comparing series of samples where only one element changes, we have identified the iron content to be the crucial parameter in stabilizing the various iron vacancy orders and the associated magnetic orders. The ratio of selenium to sulfur, on the other hand, does not affect the formation of these phases, but is important for the emergence of superconductivity. Our studies have clearly shown that the stripe AF order, the block AF order, and the SC or metallic phase in the $\text{Rb}_x\text{Fe}_y\text{Se}_{2-z}\text{S}_z$ system have distinct lattice constants and are well separated in iron content by the existence of miscibility gaps. The relationship between these phases is clearly different from that between the AF phase and the SC phase in iron pnictides, where the AF order and the superconductivity can microscopically coexist⁹, as there does not appear to be a continuous path that connects these magnetic phases to the superconducting phase. The existence of the miscibility gaps is a key to understanding the relationship between the various phases and, therefore, truly necessary ingredients for superconductivity in these rich and interesting materials.

VI. ACKNOWLEDGMENTS

This work was supported by the Director, Office of Science, Office of Basic Energy Sciences, U.S. Department of Energy, under Contract No. DE-AC02-05CH11231 and

the Office of Basic Energy Sciences U.S. DOE Grant No. DE-AC03-76SF008. The research at Oak Ridge National Laboratory's High-Flux Isotope Reactor is sponsored by the Scientific User Facilities Division, Office of Basic Energy Sciences, U.S. Department of Energy.

-
- * Electronic address: wangm@berkeley.edu
- ¹ F.-C. Hsu, J.-Y. Luo, K.-W. Yeh, T.-K. Chen, T.-W. Huang, P. M. Wu, Y.-C. Lee, Y.-L. Huang, Y.-Y. Chu, D.-C. Yan, et al., *Proc. Natl. Acad. Sci.* **105**, 14262 (2008).
 - ² S. Medvedev, T. M. McQueen, I. a. Troyan, T. Palasyuk, M. I. Eremets, R. J. Cava, S. Naghavi, F. Casper, V. Ksenofontov, G. Wortmann, et al., *Nat. Mater.* **8**, 630 (2009).
 - ³ J.-F. Ge, Z.-L. Liu, C. Liu, C.-L. Gao, D. Qian, Q.-K. Xue, Y. Liu, and J.-F. Jia, *Nat. Mater.* **14**, 285 (2014).
 - ⁴ J. Guo, S. Jin, G. Wang, S. Wang, K. Zhu, T. Zhou, M. He, and X. Chen, *Phys. Rev. B* **82**, 180520(R) (2010).
 - ⁵ M. Burrard-Lucas, D. G. Free, S. J. Sedlmaier, J. D. Wright, S. J. Cassidy, Y. Hara, A. J. Corkett, T. Lancaster, P. J. Baker, S. J. Blundell, et al., *Nat. Mater.* **12**, 15 (2012).
 - ⁶ T. P. Ying, X. L. Chen, G. Wang, S. F. Jin, T. T. Zhou, X. F. Lai, H. Zhang, and W. Y. Wang, *Sci. Rep.* **2**, 426 (2012).
 - ⁷ X. F. Lu, N. Z. Wang, G. H. Zhang, X. G. Luo, Z. M. Ma, B. Lei, F. Q. Huang, and X. H. Chen, *Phys. Rev. B* **89**, 020507(R) (2014).
 - ⁸ D. C. Johnston, *Advances in Physics* **59**, 803 (2010).
 - ⁹ G. R. Stewart, *Rev. Mod. Phys.* **83** (2011).
 - ¹⁰ W. Bao, Q. Huang, G. F. Chen, M. a. Green, D. M. Wang, J. B. He, X. Q. Wang, and Y. Qiu, *Chin. Phys. Lett.* **28**, 086104 (2011).
 - ¹¹ A. Ricci, N. Poccia, B. Joseph, G. Arrighetti, L. Barba, J. Plaisier, G. Campi, Y. Mizuguchi, H. Takeya, Y. Takano, et al., *Supercond. Sci. Technol.* **24**, 082002 (2011).
 - ¹² F. Chen, M. Xu, Q. Q. Ge, Y. Zhang, Z. R. Ye, L. X. Yang, J. Jiang, B. P. Xie, R. C. Che, M. Zhang, et al., *Phys. Rev. X* **1**, 021020 (2011).
 - ¹³ Z. Wang, Z. Wang, Y.-J. Song, C. Ma, Y. Cai, Z. Chen, H.-F. Tian, H.-X. Yang, G.-F. Chen, and J.-Q. Li, *J. Phys. Chem. C* **116**, 17847 (2012).
 - ¹⁴ V. Ksenofontov, G. Wortmann, S. Medvedev, V. Tsurkan, J. Deisenhofer, A. Loidl, and C. Felser, *Phys. Rev. B* **84**, 180508(R) (2011).
 - ¹⁵ R. H. Yuan, T. Dong, Y. J. Song, P. Zheng, G. F. Chen, J. P. Hu, J. Q. Li, and N. L. Wang, *Sci. Rep.* **2**, 221 (2012).
 - ¹⁶ A. Charukha, A. Cvitkovic, T. Prokscha, D. Pröpper, N. Ocelic, A. Suter, Z. Salman, E. Morenzoni, J. Deisenhofer, V. Tsurkan, et al., *Phys. Rev. Lett.* **109**, 017003 (2012).
 - ¹⁷ Y. Texier, J. Deisenhofer, V. Tsurkan, A. Loidl, D. S. Inosov, G. Friemel, and J. Bobroff, *Phys. Rev. Lett.* **108**, 237002 (2012).
 - ¹⁸ W. Li, H. Ding, Z. Li, P. Deng, K. Chang, K. He, S. Ji, L. Wang, X. Ma, J. P. Hu, et al., *Phys. Rev. Lett.* **109**, 057003 (2012).
 - ¹⁹ D. P. Shoemaker, D. Y. Chung, H. Claus, M. C. Francisco, S. Avci, A. Llobet, and M. G. Kanatzidis, *Phys. Rev. B* **86**, 184511 (2012).
 - ²⁰ P. Gao, R. Yu, L. Sun, H. Wang, Z. Wang, Q. Wu, M. Fang, G. Chen, J. Guo, C. Zhang, et al., *Phys. Rev. B* **89**, 094514 (2014).
 - ²¹ F. Ye, W. Bao, S.-X. Chi, M.-H. Fang, H.-D. Wang, Q.-H. Mao, J.-C. Wang, J.-J. Liu, J.-M. Sheng, A. M. D. Santos, et al., *Chin. Phys. Lett.* **31**, 127401 (2014).
 - ²² S. V. Carr, D. Louca, J. Siewenie, Q. Huang, A. Wang, X. Chen, and P. Dai, *Phys. Rev. B* **89**, 134509 (2014).
 - ²³ Y. Kobayashi, S. Kototani, K. Ohishi, and M. Itoh, *J. Phys. Soc. Jpn.* **84**, 044710 (2015).
 - ²⁴ J. Zhao, H. Cao, E. Bourret-Courchesne, D. H. Lee, and R. J. Birgeneau, *Phys. Rev. Lett.* **109**, 267003 (2012).
 - ²⁵ X. Ding, D. Fang, Z. Wang, H. Yang, J. Liu, Q. Deng, G. Ma, C. Meng, Y. Hu, and H.-H. Wen, *Nat. Comm.* **4**, 1897 (2013).
 - ²⁶ D. Gu, L. Sun, Q. Wu, C. Zhang, J. Guo, P. Gao, Y. Wu, X. Dong, X. Dai, and Z. Zhao, *Phys. Rev. B* **85**, 174523 (2012).
 - ²⁷ Z. Wang, Y. Cai, Z. W. Wang, Z. a. Sun, H. X. Yang, H. F. Tian, C. Ma, B. Zhang, and J. Q. Li, *Europhys. Lett.* **102**, 37010 (2013).
 - ²⁸ Y. J. Yan, M. Zhang, a. F. Wang, J. J. Ying, Z. Y. Li, W. Qin, X. G. Luo, J. Q. Li, J. Hu, and X. H. Chen, *Sci. Rep.* **2**, 212 (2012).
 - ²⁹ E. Dagotto, *Rev. Mod. Phys.* **85**, 849 (2013).
 - ³⁰ M. Wang, W. Tian, P. Valdivia, S. Chi, E. Bourret-Courchesne, P. Dai, and R. J. Birgeneau, *Phys. Rev. B* **90**, 125148 (2014).
 - ³¹ M. Wang, M. Wang, G. N. Li, Q. Huang, C. H. Li, G. T. Tan, C. L. Zhang, H. Cao, W. Tian, Y. Zhao, et al., *Phys. Rev. B* **84**, 094504 (2011).
 - ³² M. Wang, M. Yi, H. Cao, C. D. Cruz, S. K. Mo, Q. Z. Huang, P. Dai, D. H. Lee, Z. X. Shen, R. J. Birgeneau, et al., *Phys. Rev. B* **92**, 121101(R) (2015).
 - ³³ D. G. Porter, E. Cemal, D. J. Voneshen, K. Refson, M. J. Gutmann, A. Bombardi, A. T. Boothroyd, A. Krzton-Maziopa, E. Pomjakushina, K. Conder, et al., *Phys. Rev. B* **91**, 144114 (2015).
 - ³⁴ M. Wang, H. Luo, M. Wang, S. Chi, J. a. Rodriguez-Rivera, D. Singh, S. Chang, J. W. Lynn, and P. Dai, *Phys. Rev. B* **83**, 094516 (2011).
 - ³⁵ M. Yi, Meng Wang, A. F. Kemper, S. -K. Mo, Z. Hussain, E. Bourret-Courchesne, A. Lanzara, M. Hashimoto, D. H. Lu, Z. -X. Shen, and R. J. Birgeneau, arXiv: p. 1505.06636 (2015).
 - ³⁶ M. Fang, H. Wang, C. Dong, Z. Li, C. Feng, J. Chen, and H. Q. Yuan, *Europhys. Lett.* **94**, 27009 (2010).
 - ³⁷ A. F. Wang, J. J. Ying, Y. J. Yan, R. H. Liu, X. G. Luo, Z. Y. Li, X. F. Wang, M. Zhang, G. J. Ye, P. Cheng, et al., *Phys. Rev. B* **83**, 060512(R) (2011).
 - ³⁸ H. Lei, M. Abeykoon, E. S. Bozin, K. Wang, J. B. Warren, and C. Petrovic, *Phys. Rev. Lett.* **107**, 137002 (2011).
 - ³⁹ M. Wang, P. Valdivia, M. Yi, J. X. Chen, W. L. Zhang, R. A. Ewings, T. G. Perring, Y. Zhao, L. W. Harriger,

- J. W. Lynn, et al., Phys. Rev. B **92**, 041109(R) (2015).
- ⁴⁰ M. Wang, C. Fang, D.-X. Yao, G. Tan, L. W. Harriger, Y. Song, T. Netherton, C. Zhang, M. Wang, M. B. Stone, et al., Nat. Comm. **2**, 580 (2011).
- ⁴¹ R. Yu, P. Goswami, Q. Si, P. Nikolic, and J.-X. Zhu, Nat. Comm. **4**, 23 (2013).
- ⁴² Y. Liu, Q. Xing, K. W. Dennis, R. W. McCallum, and T. a. Lograsso, Phys. Rev. B **86**, 144507 (2012).
- ⁴³ A. Ricci, N. Poccia, G. Campi, B. Joseph, G. Arrighetti, L. Barba, M. Reynolds, M. Burghammer, H. Takeya, Y. Mizuguchi, et al., Phys. Rev. B **84**, 060511(R) (2011).
- ⁴⁴ F. Han, H. Yang, B. Shen, Z.-Y. Wang, C.-H. Li, and H.-H. Wen, Philos. Mag. **92**, 2553 (2012).